

# Diborane Interactions with Pt<sub>7</sub>/Alumina: Preparation of Size-Controlled Borated Pt Model Catalysts

Eric T. Baxter,<sup>†</sup> Mai-Anh Ha,<sup>‡</sup> Ashley C. Cass,<sup>†</sup> Huanchen Zhai,<sup>‡</sup> Anastassia N. Alexandrova,<sup>\*,‡,§,ID</sup> and Scott L. Anderson<sup>\*,†,ID</sup>

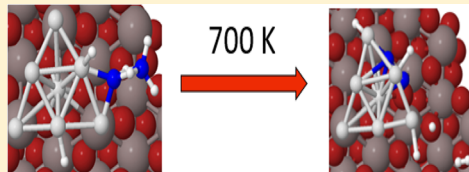
<sup>†</sup>Department of Chemistry, University of Utah, Salt Lake City, Utah 84112, United States

<sup>‡</sup>Department of Chemistry & Biochemistry, University of California, Los Angeles, Los Angeles, California 90095, United States

<sup>§</sup>California NanoSystems Institute, Los Angeles, California 90095, United States

## S Supporting Information

**ABSTRACT:** Bimetallic catalysts provide the ability to tune catalytic activity, selectivity, and stability. Model catalysts with size-selected bimetallic clusters on well-defined supports offer a useful platform for studying catalytic mechanisms; however, producing size-selected bimetallic clusters can be challenging. In this study, we present a way to prepare bimetallic model (Pt<sub>n</sub>B<sub>m</sub>/alumina) cluster catalysts by depositing size-selected Pt<sub>7</sub> clusters on an alumina thin film, then selectively adding boron by exposure to diborane, and heating. The interactions between Pt<sub>7</sub>/alumina and diborane were probed using temperature-programmed desorption/reaction (TPD/R), X-ray photoelectron spectroscopy (XPS), low-energy ion scattering (ISS), plane wave density functional theory (PW-DFT), and molecular dynamic (MD) simulations. It was found that the diborane exposure/heating process does result in preferential binding of B in association with the Pt clusters. Borated Pt clusters are of interest because they are known to exhibit reduced affinity to carbon deposition in catalytic dehydrogenation. At high temperatures, theory, in agreement with experiment, shows that boron tends to migrate to sites beneath the Pt clusters, forming Pt–B–O<sub>surf</sub> bonds that anchor the clusters to the alumina support.



## I. INTRODUCTION

Carbon deposition (i.e., “coking”) leads to deactivation of catalysts in important reactions such as Fischer–Tropsch synthesis,<sup>1</sup> hydrocarbon cracking,<sup>2</sup> and alkene dehydrogenation.<sup>3</sup> It has been demonstrated that boration of extended surfaces of Co<sup>4</sup> and Ni<sup>5</sup> can extend the lifetime of catalysts without compromising their activity toward Fischer–Tropsch synthesis and steam reforming, respectively. In both processes, coking is the mechanism of deactivation. We recently showed that boration also reduces coking on size-selected Pt clusters deposited on alumina during dehydrogenation of alkenes.<sup>6</sup> This type of catalytic system is novel and so far largely under-investigated, including several aspects of their preparation, experimental characterization, theoretical analysis, and structural, dynamical, and chemical properties.

Model catalysts with atomically size-selected clusters on well-characterized supports provide a useful platform for studying catalysis mechanisms, allowing independent control of the size and density of catalytic sites and facilitating detailed theoretical studies. Bimetallic catalysts provide important opportunities to tune catalytic activity, selectivity, and stability. However, extending the size-selected model catalyst approach to bimetallic clusters is challenging. One approach is to use alloy or dual target cluster sources that directly produce bimetallic clusters in the gas phase, which can then be mass selected and deposited to create bimetallic model catalysts.<sup>7–10</sup> This approach is quite general, in principle; however, for several

reasons it becomes increasingly difficult as the cluster size increases. The cluster source intensity is “diluted” over an increasing number of possible M<sub>x</sub>N<sub>y</sub> combinations, and the intensity is further decreased by the need for high mass-selector resolution to separate closely spaced masses. Intensity is important because clusters quickly become contaminated due to substrate-mediated adsorption,<sup>11–13</sup> even in ultrahigh vacuum (UHV). In many cases, natural isotope distributions exacerbate these problems such that clean selection of both size and composition may be impossible except for very small clusters. For example, Pt has *major* isotopes with atomic masses 194, 195, 196, and 198, and boron has isotopes with atomic masses 10 and 11. Thus, even for clusters containing only three Pt atoms, the width of the Pt isotopologue distribution is greater than the boron mass, resulting in mass overlaps between Pt<sub>3</sub>B<sub>n</sub> and Pt<sub>3</sub>B<sub>n±1</sub>.

One motivation for this paper is to report a complementary approach to producing size-selected bimetallic cluster catalysts, in which mass-selected cluster deposition is used to create a size-selected model catalyst (here, Pt<sub>n</sub>/alumina), which is then used to seed deposition of a second element to create a bimetallic model catalyst (here, Pt<sub>n</sub>B<sub>m</sub>/alumina). The challenge is to find conditions where boron deposits only on the Pt

Received: October 20, 2017

Revised: December 6, 2017

Published: December 20, 2017

clusters and then to characterize the nature of the resulting doped clusters.

## II. METHODS

As outlined below, alumina-supported size-selected  $\text{Pt}_{4,7,8}$  model catalysts were prepared, then exposed to diborane, and heated to drive decomposition and  $\text{H}_2$  desorption. The goal is to selectively borate the Pt clusters; thus, it is important to understand how diborane interacts with both  $\text{Pt}_n$  clusters and the alumina support. These interactions were probed by temperature-programmed desorption and reaction (TPD/R), low-energy  $\text{He}^+$  ion scattering (ISS), and X-ray photoelectron spectroscopy (XPS) experiments on both Pt-free alumina and  $\text{Pt}_n/\text{alumina}$  samples, by plane wave density functional theory (PW-DFT) calculations of adsorption geometries and energetics, and by molecular dynamic (MD) simulations of borane surface chemistry. We previously showed that the chemical consequences of boration are similar for different Pt cluster sizes.<sup>6</sup> Here we focus on the boration mechanism, using  $\text{Pt}_7/\text{alumina}$  as the example system.

**Computations.** As discussed previously in detail,<sup>14</sup> PW-DFT calculations with projector augmented wave potentials<sup>15,16</sup> and the PBE<sup>17</sup> functional were implemented in the Vienna Ab initio Simulation Package (VASP).<sup>18–21</sup> The bulk-optimized unit cell of  $\alpha$ -alumina with lattice constants of  $a = 4.807 \text{ \AA}$  and  $c = 13.126 \text{ \AA}$  was grown to a  $(3 \times 3)$  surface, a slight expansion as compared to experiment.<sup>22,23</sup> A vacuum gap of  $15 \text{ \AA}$  was added to the slab. The bottom half of the surface was kept fixed. For all calculations, convergence criteria of  $10^{-5}$  ( $10^{-6}$ ) eV for geometric (electronic) relaxations, expansion of the plane waves' kinetic energy to 400.0 eV, and a k-point grid of  $1 \times 1 \times 1$  centered at the  $\Gamma$ -point were instituted. We previously discussed the global optimization of  $\text{Pt}_7$  on the model  $\alpha$ -alumina surface,<sup>14</sup> finding a number of low-lying isomers for  $\text{Pt}_7/\text{alumina}$ . As shown below, the global minimum has  $\text{Pt}_7$  in a prismatic (i.e., 3D) structure with  $\text{Pt}_7$ –alumina adsorption energy of  $-5.09 \text{ eV}$ ; however, there are isomers only  $0.05 \text{ eV}$  higher in energy in which all Pt atoms are in a single layer bound to the alumina surface.

A *per manum* search for diborane adsorption geometries associated with both the prismatic and single layer  $\text{Pt}_7/\text{alumina}$  structures was made, starting with the molecule positioned at bridging, hollow, and atomic (atop) sites, oriented both parallel and normal to the surface plane and rotated in various orientations. The starting geometries focused on adsorption of diborane to the Pt clusters rather than to the  $\alpha\text{-Al}_2\text{O}_3$  surface. The adsorption energy of diborane was calculated via the relation

$$E_{\text{B}_2\text{H}_6} = E[\text{Surf} + \text{Pt}_7\text{-B}_2\text{H}_6] - E[\text{B}_2\text{H}_6]_{\text{gas}} - E[\text{Surf} + \text{Pt}_7\text{,glob}]$$

*Ab initio* MD calculations, starting at the lowest minimum of diborane adsorbed on both the prismatic and single-layer  $\text{Pt}_7/\text{alumina}$  structures, were also performed. Equilibration of the system utilized the Nosé–Hoover thermostat<sup>24</sup> and an electronic convergence criterion of  $10^{-8} \text{ eV}$  per 1 fs time-step was implemented. The global optimization of  $\text{Pt}_4\text{B}_4$  adsorbed on alumina was performed using the basin hopping method adapted for surface deposited clusters.<sup>25</sup> The local minima search for gas phase  $\text{Pt}_4\text{B}_4$  also utilized basin hopping. The adsorption energy of  $\text{Pt}_4\text{B}_4$  was taken as

$$E_{\text{ads}} = E[\text{Surf} + \text{Pt}_4\text{B}_4] - E[\text{Pt}_4\text{B}_4]_{\text{gas,glob}} - E[\text{Surf}]$$

**Experiments.** The experiments were conducted with an instrument consisting of a mass-selected metal cluster ion deposition beamline<sup>26</sup> that terminates in an ultrahigh vacuum ( $\sim 1.5 \times 10^{-10} \text{ Torr}$ ) analysis chamber that allows *in situ* sample preparation and characterization, as discussed previously, along with several of the experimental protocols used here.<sup>12,25,28</sup> The  $\text{Pt}_n/\text{alumina}$  model catalysts were prepared on a  $7 \times 7 \text{ mm}$   $\text{Ta}(110)$  single crystal mounted using Ta heating wires to a liquid nitrogen reservoir at the end of a manipulator. The sample temperature was controlled between 110 and  $>2100 \text{ K}$  by the combination of resistive and electron-bombardment heating and liquid nitrogen cooling. Temperature was measured by a C-type thermocouple spot-welded to the back of the Ta single crystal.

Procedures for alumina film growth were adapted from the Goodman<sup>29–31</sup> and Madey<sup>32,33</sup> groups. At the beginning of each experiment, the Ta single crystal was annealed above 2100 K for 5 min or until no surface contaminants were detected by XPS and ISS. For alumina film growth, the  $\text{Ta}(110)$  substrate was transferred to a separately pumped UHV antechamber and heated to 970 K in  $5 \times 10^{-6} \text{ Torr}$  of  $\text{O}_2$ , while exposed to Al evaporating from a crucible mounted normal to the  $\text{Ta}(110)$  surface. In previous studies,<sup>28,34</sup> we demonstrated that the reactivity, adsorbate binding, and electronic properties of Pd clusters deposited on alumina were independent of film thickness in the 3–10 nm range. For these studies, the typical growth rate was  $\sim 0.2 \text{ nm/min}$  and 3–6 nm thick films were used.

Before beginning cluster deposition, the alumina/ $\text{Ta}(110)$  support was flashed to  $\sim 800 \text{ K}$  to desorb adventitious adsorbates. To minimize the time the clusters were exposed to background gases, Pt cluster deposition was done as the sample cooled after the flash, beginning when the sample reached  $\sim 300 \text{ K}$ . The clusters were deposited onto the alumina support through a 2 mm diameter mask, and cluster coverage was controlled by monitoring the neutralization current of soft landed ( $\sim 1 \text{ eV/atom}$ ) clusters on the support. Unless stated otherwise, all samples were prepared with  $\text{Pt}_7$  coverage of  $2.14 \times 10^{13} \text{ clusters/cm}^2$ , amounting to  $1.5 \times 10^{14} \text{ Pt atoms/cm}^2$ , equivalent to  $\sim 10\%$  of a close-packed Pt monolayer.

TPD/R measurements were made using a differentially pumped mass spectrometer that views the main UHV chamber through the  $\sim 2.5 \text{ mm}$  diameter aperture in a skimmer cone. The cone was surrounded by four directional dose tubes that pointed at the sample position, and gas doses for both TPD/R and diborane exposure were done using the tubes to minimize gas exposures to the vacuum system. To calibrate the exposures, we compared subsaturation CO TPD signals for CO delivered through the dose tubes and through a gas inlet remote from the sample position. During both gas dosing and the subsequent TPD/R heat ramp, the chamber pressure was monitored by a nude ion gauge, and ion signals of interest were measured by the differentially pumped mass spectrometer. The analyte molecules were ionized by electron impact ionization (EI) using electrons with a nominal energy of 65 eV. This energy was found to give the best intensity for  $\text{D}_2$  and  $\text{C}_2\text{D}_4$  detection. Diborane TPD/R was done by exposing samples to  $\text{B}_2\text{H}_6$  at 130 K sample temperature, followed by heating to 700 K. For ethylene TPD/R, the sample was exposed to 5 langmuirs of  $\text{C}_2\text{D}_4$  at a sample temperature of 150 K (to minimize multilayer adsorption), cooled to 130 K, and then heated to 700 K while monitoring signals for  $\text{C}_2\text{D}_4^+$ ,  $\text{D}_2^+$ , and various background gases.

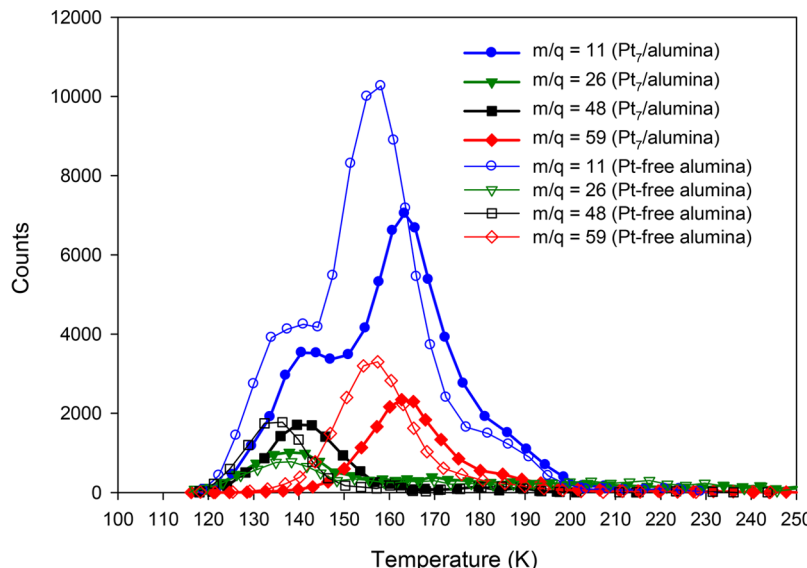


**Figure 1.** TPD spectra for select ion signals, corrected for EI cracking of borane species. Alumina and Pt<sub>7</sub>/alumina samples were exposed to 1.5 langmuirs of diborane at 130 K and then heated at 3 K/s while monitoring desorption mass spectrometrically.

Boron was introduced into the UHV system in the form of a diborane/argon gas mixture that we characterized mass spectrometrically to have actual composition of 4.8% diborane, 85% argon, and 10.2% H<sub>2</sub>, the latter assumed to result from diborane decomposition during storage.<sup>35</sup> Diborane exposures were calculated based on the measured diborane mole fraction. In most experiments, boration was done by exposing the samples to 1.5 langmuirs of diborane at a sample temperature of 130 K, followed by heating to 700 K, which was found to be sufficient to drive desorption to completion. Note that a 1.5 langmuir diborane exposure corresponds to  $\sim 5.8 \times 10^{14}$  diborane molecules impinging per cm<sup>2</sup>, i.e., smaller than the total number of surface atoms, but almost 4 times larger than the number of Pt atoms. A few experiments were performed using a 0.5 langmuir diborane exposure, where the number of impinging diborane molecules ( $1.9 \times 10^{14}/\text{cm}^2$ ) was only  $\sim 25\%$  greater than the number of Pt atoms present. The dose variation had little effect on the sample properties, suggesting that 1.5 langmuirs should be more than sufficient to saturate the Pt cluster binding sites.

Because the gas mixture contained hydrogen, and diborane decomposition also produces hydrogen, we studied TPD following pure D<sub>2</sub> exposure, in separate experiments. H<sub>2</sub> desorption during diborane TPD/R could not be monitored because the mass 2 background in the mass spectrometer was too high.

XPS (Al K $\alpha$ ) was used to examine both alumina and Pt<sub>7</sub>/alumina samples after B<sub>2</sub>H<sub>6</sub> exposure, both while holding the sample at the 130 K dose temperature, and after heating the sample to 700 K. Since both boron and Pt are present only in the surface layer, and we know the Pt coverage quite precisely, the boron coverage was estimated from the ratio of B 1s and Pt 4d XPS integrated intensities. The Pt 4d XPS signal was used because of overlap between Pt 4f and Al 2p. Both Pt and B are present at low coverage, and because the B 1s photoemission cross section is  $\sim 40$  times smaller than that for Pt 4d,<sup>36</sup> the boron XPS signal is quite weak. To improve the signal/noise, the boron XPS measurements were done using samples with double the normal Pt<sub>n</sub> coverage (i.e., 0.2 ML). Higher cluster coverage undoubtedly resulted in some increase in cluster

agglomeration during deposition and heating; however, because the effects of boration do not appear to be very dependent on cluster size,<sup>6</sup> a modest degree of agglomeration is unlikely to have a significant effect on the B/Pt ratio. To ensure that the diborane exposure was sufficient to saturate the larger number of Pt<sub>7</sub> present, we also doubled the diborane dose to 3.0 langmuirs.

For ISS, a beam of 1 keV He<sup>+</sup> was loosely focused onto the surface at 45° angle of incidence, and the energy distribution of He<sup>+</sup> scattered along the surface normal was measured. Peaks in ISS result from scattering of He<sup>+</sup> from single atoms in the sample, predominantly in the surface layer.<sup>37</sup> Multiple scattering and scattering from subsurface layers contribute primarily to a weak background. In these experiments, ISS was used to monitor the intensities associated with Pt, Al, and O atoms in the top sample layer. H is undetectable by ISS, and the boron ISS signal also proved to be undetectable due to the combination of low He<sup>+</sup> scattering cross section ( $\sigma_{\text{scatt}} \propto Z_{\text{target}}$ ), low boron coverage, and rising background in that energy range from multiple scattering. Because ISS is a destructive technique, the ISS experiments were done either on separately prepared samples or at the end of other experimental sequences.

### III. RESULTS

**Temperature-Programmed Desorption/Reaction Following Adsorption of B<sub>2</sub>H<sub>6</sub> and D<sub>2</sub>.** TPD/R experiments were used to identify species desorbing from alumina and Pt<sub>7</sub>/alumina surfaces and the associated temperature dependences (i.e., energetics). Because the literature shows that diborane can polymerize on surfaces,<sup>38</sup> we monitored masses relevant to known boranes of various sizes. Figure S1 in the Supporting Information shows the raw TPD signals for ion masses 11, 26, 48, and 59, which are low background masses corresponding to B<sub>1</sub>H<sub>x</sub><sup>+</sup>, B<sub>2</sub>H<sub>x</sub><sup>+</sup>, B<sub>4</sub>H<sub>x</sub><sup>+</sup>, and B<sub>5</sub>H<sub>x</sub><sup>+</sup> (the <sup>11</sup>B:<sup>10</sup>B isotope ratio is  $\sim 80:20$ ). Figure 1 shows the data corrected for the estimated contributions from fragmentation of higher boranes during electron impact ionization (EI) at 65 eV. The assignment of the ion signals to desorbing species is complicated by the fact that boranes fragment extensively in EI.<sup>39</sup> We corrected the TPD signals for fragmentation of diborane, tetraborane (B<sub>4</sub>H<sub>10</sub>) and

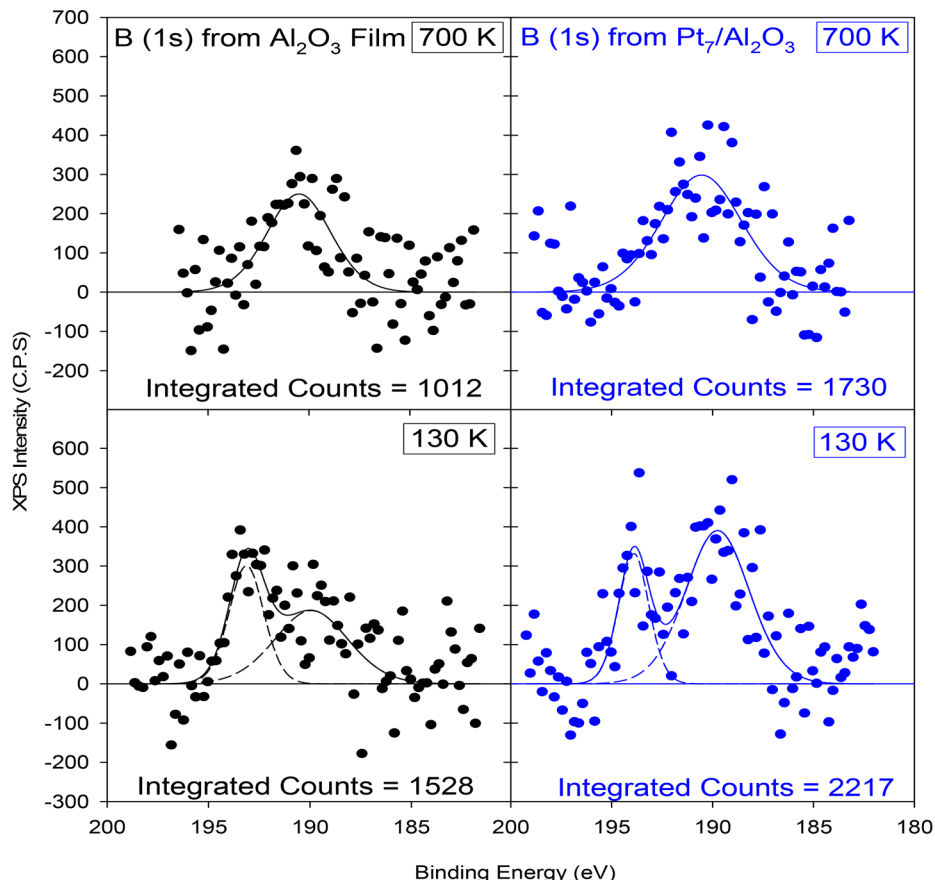


**Figure 2.** XPS spectra obtained for both Pt-free alumina (black) and Pt<sub>7</sub>/alumina (blue) samples following exposure to 3 langmuirs of B<sub>2</sub>H<sub>6</sub> at 130 K and after heating to 700 K.

pentaborane (B<sub>5</sub>H<sub>9</sub>), which all have tabulated standard EI mass spectra, but did not attempt to correct for possible contributions from higher boranes (i.e., B<sub>n</sub>H<sub>m</sub>,  $n > 5$ ) or from boranes which could conceivably be generated by desorption, but for which standard mass spectra are unavailable. In addition, ion fragmentation is sensitive to the internal energy of the neutral molecules; thus, there may be errors in comparing room temperature standard spectra with those for boranes desorbing below room temperature. For all these reasons, we regard the correction of the measured TPD/R data as useful but qualitative. Fortunately, as can be seen by comparing Figure 1 and Figure S1, the corrections are quite small. Further discussion of the analysis can be found in the Supporting Information.

Data are shown for desorption from both alumina and Pt<sub>7</sub>/alumina samples, each exposed to 1.5 langmuirs of B<sub>2</sub>H<sub>6</sub> at 130 K and then heated at 3 K/s. Note that desorption starts at ~120 K, i.e., slightly below the dose temperature. This reflects the fact that diborane pumps out of the system slowly, so that there was a small additional exposure as the sample cooled to the TPD/R start temperature.

One surprise is that the mass 11 signal (<sup>11</sup>B<sup>+</sup> and <sup>10</sup>BH<sup>+</sup>) is quite high, even after subtraction of the expected contributions from EI fragmentation of di-, tetra-, and pentaborane. We considered the possibility that the high mass 11 intensity might be an artifact of high mass spectrometer sensitivity to light masses, but this explanation is ruled out by the excellent agreement of our mass spectrum for diborane with the NIST standard diborane spectrum.<sup>39</sup> For example, when we leak

diborane into our UHV system, we measure a mass 11:26 intensity ratio of ~0.3:1, in good agreement with the 0.28:1 ratio reported in the NIST database. It is also unlikely that the high mass 11 signal could result from EI fragmentation of higher boranes (B<sub>n</sub>H<sub>m</sub>,  $n \geq 6$ ) because these, if present in high enough yield to account for such high mass 11 signal, would also result in much higher mass 59 signal than is observed.

Therefore, we conclude that the high mass 11 signal must largely result from desorption of some BH<sub>x</sub> species, such as borane (BH<sub>3</sub>). Diborane is a hydrogen-bridge-bonded dimer, with gas-phase dissociation enthalpy to 2 BH<sub>3</sub> of only 1.78 eV (i.e., 0.89 eV/BH<sub>3</sub>),<sup>40</sup> and both BH<sub>3</sub> and BH<sub>2</sub> are detected mass spectrometrically in gas-phase pyrolysis of diborane at 300 °C.<sup>41</sup> We observe mass 11 desorption signal at low temperatures, raising the question of how BH<sub>2</sub> or BH<sub>3</sub> production is energetically feasible. For reactions of diborane on a surface, the energy required to generate gas-phase BH<sub>x</sub> may be supplied by recombination reactions (e.g., producing tetra- and pentaborane) or by formation of strong B–surface bonds.

Diborane surface chemistry will be discussed in more detail after the rest of the experimental and theoretical results are presented. The most important points to keep in mind are: (1) Because all boranes fragment in EI to produce at least some mass 11, the absence of mass 11 signal above ~200 K implies that desorption of boron-containing species is complete by 200 K. (2) The mass 11 signal is far too large to be explained by EI fragmentation of B<sub>n</sub>H<sub>m</sub> ( $n \geq 2$ ), implying that there is considerable desorption of BH<sub>x</sub>. (3) The fact that masses 11, 48, and 59 are observed with higher intensities than mass 26

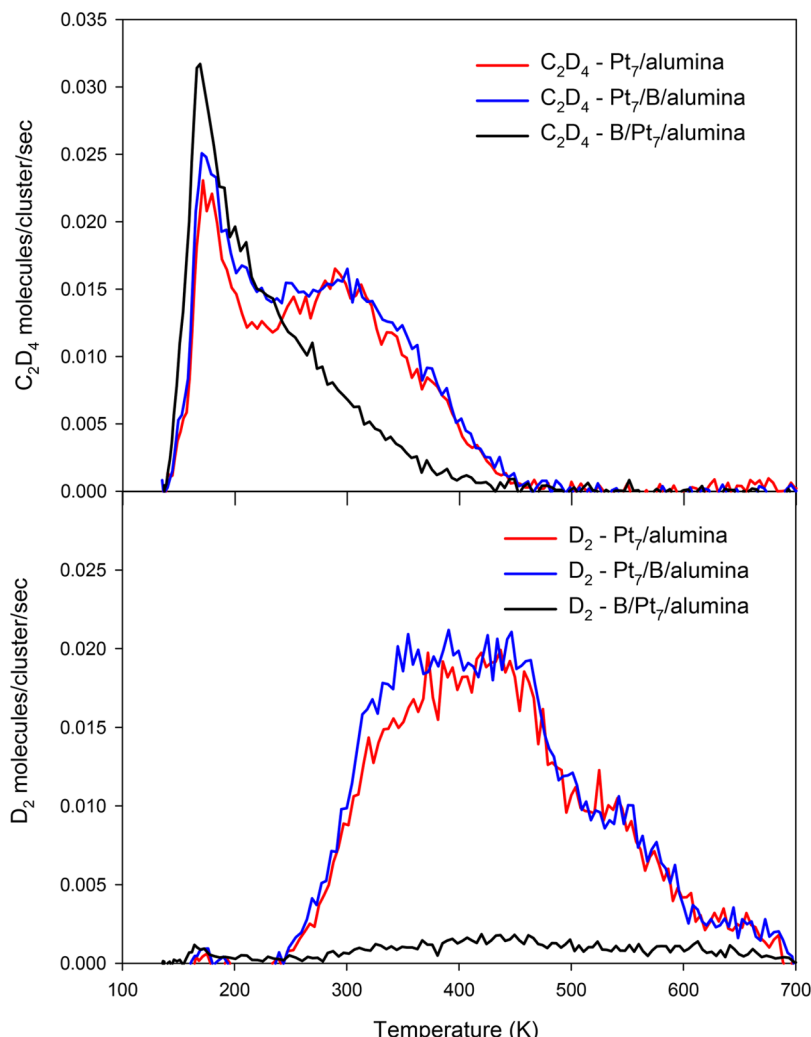


**Figure 3.** Thermal desorption spectra of unreacted ethylene and deuterium product obtained from three samples: (red) as-deposited  $\text{Pt}_7/\text{alumina}$  with no boron exposure, (blue)  $\text{Pt}_7$  deposited on preborated alumina, and (black)  $\text{Pt}_7/\text{alumina}$  borated after  $\text{Pt}_7$  deposition. Each sample was exposed to 5 langmuirs of  $\text{C}_2\text{D}_4$  at 150 K. Boration was done using our standard method (1.5 langmuirs of  $\text{B}_2\text{H}_6$  at 130 K, heating to 700 K). Separate samples were used for each experiment.

implies that most of the desorbing boron fraction is in the form of reaction products rather than diborane. (4) Desorptions from alumina and  $\text{Pt}_7/\text{alumina}$  are qualitatively similar, as might be expected, considering that 90% of the  $\text{Pt}_7/\text{alumina}$  surface is alumina. (5) The total amount of  $\text{B}_n\text{H}_m$  desorption is ~13% lower when  $\text{Pt}_7$  is present at 10% coverage, and the desorption peaks are shifted 5–10 K to higher temperatures.

Species such as  $\text{B}_4\text{H}_{10}$  and  $\text{B}_5\text{H}_9$  have the H:B ratios that are smaller than that for diborane (3:1). In addition, the XPS results discussed next show that a significant amount of boron remains on the surface after  $\text{B}_n\text{H}_m$  desorption has gone to completion. It is clear, therefore, that hydrogen must also be desorbing during diborane TPD/R. Observation of the diborane  $\rightarrow \text{H}_2$  desorption channel is not possible, both because the mass 2 background is high and because the diborane reactant gas mixture has substantial  $\text{H}_2$  concentration. To provide some insight into the binding/desorption behavior of hydrogen on  $\text{Pt}_7/\text{alumina}$ , we measured  $\text{D}_2$  desorption from a separate  $\text{Pt}_7/\text{alumina}$  sample dosed with 5 langmuirs of  $\text{D}_2$  at 130 K, and the result is shown in Figure S5. A small amount of  $\text{D}_2$  desorption is observed in the temperature range below ~200 K, where borane desorption occurs, but ~90% of

hydrogen desorption occurs at higher temperatures, between 200 and 400 K.

We estimated desorption energies for the different species by fitting the TPD/R temperature dependence to a second-order kinetic model, i.e., assuming that the rate-limiting step is recombination of adsorbed  $\text{B}_n\text{H}_m$  fragments to generate the various boranes observed. The desorption energy distributions are shown in Figures S2 and S3, and the desorption energies all fall in the 0.4–0.5 eV range.

**X-ray Photoelectron Spectroscopy.** TPD/R probes the  $\text{B}_n\text{H}_m$  species that desorb upon heating, but from the perspective of selectively borating the Pt clusters, it is more important to understand the fate of the boron that remains on the surface. XPS was used to probe the fraction of B on the samples before and after heating. Figure 2 compares B 1s spectra for both alumina and  $\text{Pt}_7/\text{alumina}$  samples, after exposure to 3 langmuirs of  $\text{B}_2\text{H}_6$  at 130 K and after subsequent heating to 700 K. As noted above, the low B 1s photoemission cross section results in poor signal, and the XPS experiments were done using a sample with  $\text{Pt}_7$  deposited at twice the normal coverage ( $\sim 3 \times 10^{14}$  Pt atoms/cm<sup>2</sup>).

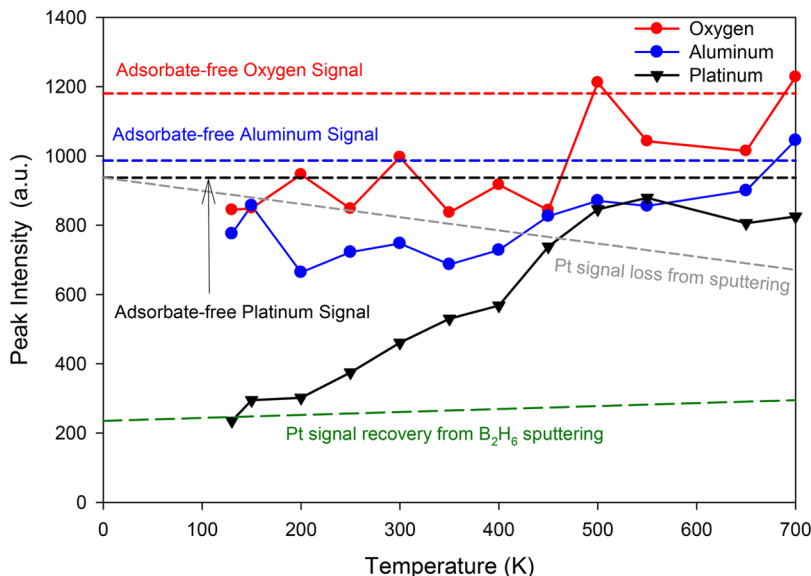


**Figure 4.** TD-ISS of Pt<sub>7</sub>/alumina exposed to 1.5 K of diborane at 110 K. The intensities for adsorbate-free Pt<sub>7</sub>/alumina, measured separately, are indicated as horizontal dashed lines. The effects of He<sup>+</sup> sputtering on Pt signal in adsorbate-free and diborane-dosed Pt<sub>7</sub>/alumina held at 110 K are shown as dashed lines labeled “Pt signal loss from sputtering” and “Pt signal recovery from B<sub>2</sub>H<sub>6</sub> sputtering”, respectively.

The B 1s XP spectrum of diborane adsorbed at 130 K on Pt<sub>7</sub>/alumina is noisy (bottom right frame) but clearly indicates the presence of two components, fit by peaks at 189.7 and 193.9 eV, suggesting the presence of at least two boron chemical environments. The 130 K spectrum for Pt-free alumina (bottom left) has similar intensity peaking near 193 eV, but the low binding energy intensity is weaker than in the Pt<sub>7</sub>/alumina sample. A similar two-component fit was used for this spectrum, resulting in peaks centered at 189.7 and 193.1 eV. After heating to 700 K, only a single broad B 1s feature remains for both alumina and Pt<sub>7</sub>/alumina, peaking at 190.5 eV binding energy.

The integrated intensities, indicated in each frame of the figure, provide additional insight into diborane interactions with alumina and Pt<sub>7</sub>. Note that the integrated B 1s intensity at 130 K, i.e., the total amount of boron adsorbed, is ~45% higher when Pt<sub>7</sub> is present. Heating to 700 K to desorb all volatile boron species leads to loss of ~34% of the initial B 1s signal for alumina, but only ~22% of the (initially larger) B 1s signal for Pt<sub>7</sub>/alumina. Thus, after heating, the amount of boron remaining on the sample is ~71% higher when Pt<sub>7</sub> is present, even though the Pt<sub>7</sub> coverage was only ~20%. This result can be compared to the TPD/R results, which showed ~13% less desorption of boron-containing species when Pt<sub>7</sub> was present (at 10% coverage). Taken together, both TPD/R and XPS show that substantially more boron adsorbs when Pt<sub>7</sub> is present but that less desorbs when heated; i.e., the presence of a low coverage of Pt<sub>7</sub> leads to substantially more boron deposition on the samples.

**Effect of Boration of Alumina vs Pt<sub>n</sub> on Ethylene TPD/R.** XPS shows that the boration process leads to some boron deposition on the alumina film support; thus, it is important to know how the catalytic properties of the samples are affected by the boron atoms on (or in) the support. To address this question, Figure 3 compares the ethylene adsorption, desorption, and dehydrogenation behavior of three samples: (1) as-deposited Pt<sub>7</sub>/alumina with no boron exposure (“Pt<sub>7</sub>/alumina”); (2) Pt<sub>7</sub>/alumina borated after cluster deposition, i.e., both Pt<sub>7</sub> and alumina with boron (“B/Pt<sub>7</sub>/alumina”); (3) Pt<sub>7</sub>

deposited on a preborated alumina support, i.e., only the alumina was borated (“Pt<sub>7</sub>/B/alumina”). Boration was done using our standard method (1.5 langmuir B<sub>2</sub>H<sub>6</sub> exposure at 130 K, followed by heating to 700 K), and ethylene TPD/R was carried out under conditions identical to those used in our previous studies<sup>6,14</sup> (5 langmuir C<sub>2</sub>D<sub>4</sub> exposure at 150 K, heating at 3 K/s to 700 K). Ethylene desorbs from Pt<sub>7</sub>/alumina in two components. The low-temperature feature was shown to result from ethylene desorbing from defect sites in the alumina film, and the broad feature peaking near 300 K results from ethylene adsorbed at Pt<sub>7</sub> sites.<sup>14</sup> A substantial amount of D<sub>2</sub> desorption is observed above 300 K for Pt<sub>7</sub>/alumina, but none is observed for the alumina film alone.

Boration of both the clusters and the support (B/Pt<sub>7</sub>/alumina) leads to a substantial decrease in the temperature distribution for ethylene desorption and near-total attenuation of D<sub>2</sub> desorption. In contrast, borating only the alumina support (Pt<sub>7</sub>/B/alumina) has little effect on the Pt<sub>7</sub> chemistry. The low-temperature ethylene desorption feature attributed to desorption from the alumina support is less intense and sharper for this sample, suggesting that boration of the alumina support weakens the ethylene–alumina binding, possibly due to boron occupying alumina defect sites. Preboration has little effect, however, on the amount or temperature dependence of ethylene desorbing from Pt sites, or on the D<sub>2</sub> production, suggesting that the presence of a small amount of boron in the support has little effect on supported Pt clusters. Clearly, the large effects of boron on chemistry of supported Pt clusters are due to boration of the Pt clusters rather than the support.

**Temperature-Dependent Ion Scattering Spectroscopy.** The final experimental probe of diborane–surface interactions was temperature-dependent He<sup>+</sup> ion scattering (TD-ISS). TD-ISS involves cooling the sample, exposing it to an adsorbate of interest, and then monitoring changes in ISS intensities as the sample is heated. A typical raw ISS scan (Figure S4) shows distinct peaks for single scattering from Pt, O, and Al atoms in the surface layer<sup>37</sup> along with a featureless background due to multiple and subsurface scattering. As discussed previously,<sup>12,14</sup> Pt<sub>7</sub> deposits in an ensemble of

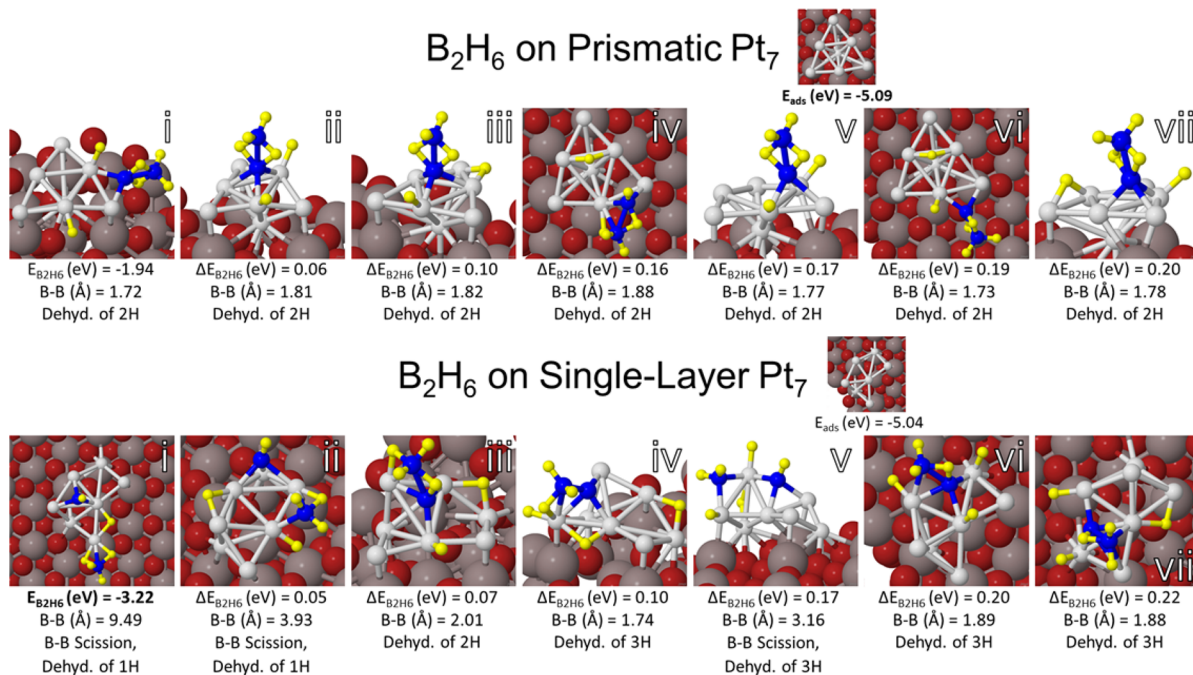


**Figure 5.** Seven lowest minima of diborane ( $\text{B}_2\text{H}_6$ ) adsorbed on the two lowest minima of  $\text{Pt}_7$ , which also represent two different structural classes of  $\text{Pt}$  clusters, i.e., “prismatic” and “single layer”. The most stable adsorbate-free  $\text{Pt}_7/\text{alumina}$  isomer is prismatic, but with diborane adsorbed the single layer isomer becomes more stable by over 1 eV. Boron atoms are depicted in blue, platinum in light gray, hydrogen in yellow, aluminum in dark gray, and oxygen in red.

prismatic and single layer structures, with most of the Pt in the surface layer and thus detectable by ISS. Adsorbates attenuate ISS signals from the underlying surface through a combination of shadowing, blocking, and reduced ion survival probability.<sup>37,42</sup> For our scattering geometry, attenuation primarily affects signal from atoms directly under, or surrounding, the adsorbate. Thus, adsorbates binding directly on top of the Pt clusters attenuate Pt signal, with little or no effect on Al or O signals. Conversely, adsorption on the alumina film, or at sites around the periphery of the clusters, tends to attenuate Al and O signals, with little or no effect on the Pt signal. As heating drives desorption, the attenuated ISS signals should tend to recover toward the adsorbate-free values. To the extent that diborane exposure and heating leads to cluster agglomeration, forming larger multilayer Pt particles, this would reduce the fraction of Pt in the surface layer and thus the Pt ISS signal.

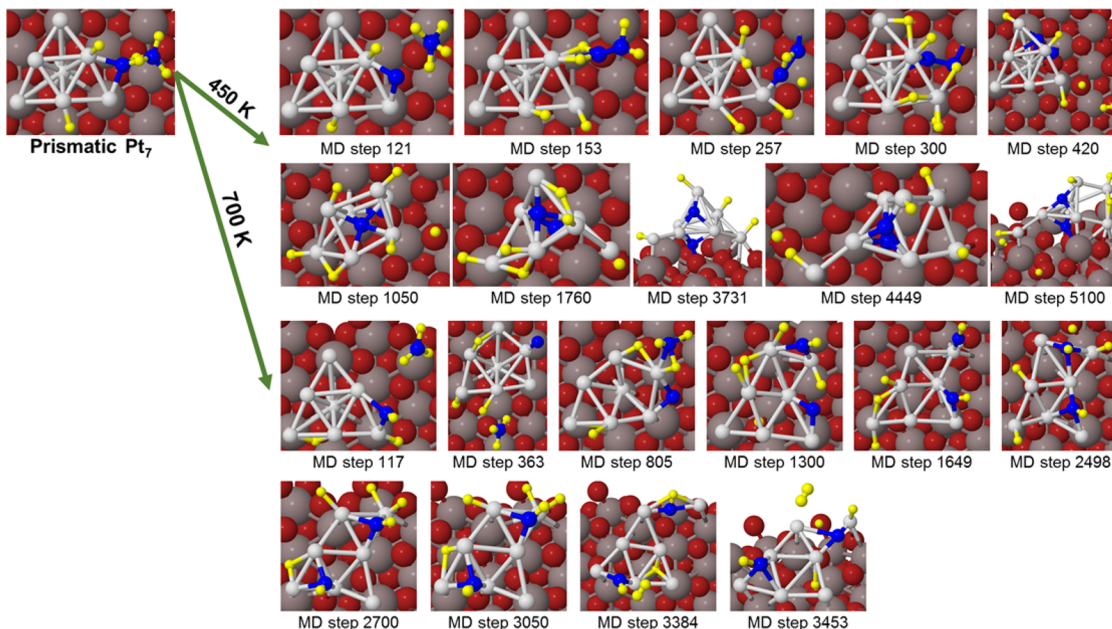
As shown in Figure S4, there is no obvious ISS signal for boron ( $E/E_0 \approx 0.26$ ) in the spectrum taken immediately after diborane exposure at 110 K, nor is B ISS signal observed after heating the sample, despite the evidence that boron must be present on these samples (Figures 1 and 2). Lack of boron signal could be taken as evidence that boron is not in the surface layer; however, boron may simply have been undetectable due to a combination of low coverage, small  $\text{He}^+$ -B scattering cross section ( $\propto$  target atomic number<sup>37</sup>), and high multiple-scattering background at low  $E/E_0$ .

Figure 4 compares the Pt, O, and Al ISS signals as a function of temperature for a  $\text{Pt}_7/\text{alumina}$  sample that was exposed to 1.5 langmuirs of  $\text{B}_2\text{H}_6$  at 110 K, probed by ISS, and then heated to 700 K in 50 K steps, with an ISS measurement made at each temperature. All spectra were collected with low ( $0.1 \mu\text{A}$ )  $\text{He}^+$  flux impinging at  $45^\circ$  and detected along the surface normal, with 30 s scan time used to minimize sample damage. The horizontal dashed lines show the Pt, O, and Al intensities

measured for adsorbate-free  $\text{Pt}_7/\text{alumina}$  in a separate experiment. Compared to these adsorbate-free values, the signals measured after the  $\text{B}_2\text{H}_6$  dose are attenuated by  $\sim 80\%$  for Pt and  $\sim 20\%$  for O and Al, indicating that  $\text{B}_2\text{H}_6$  binds preferentially in sites that attenuate Pt ISS signal. ISS, thus, is consistent with the XPS and TPD/R results indicating that diborane binds preferentially in association with  $\text{Pt}_7$  and provides the additional insight that some or all of this Pt-associated diborane binds on top of the clusters, where it attenuates scattering from underlying Pt. The  $\sim 20\%$  attenuation of Al and O signals indicates that some diborane binds in sites that shadow or block scattering from alumina, which could include both sites around the periphery of the clusters and on the alumina film remote from the clusters.

Interpretation of changes in signal as the sample is heated requires knowledge of the effects of  $\text{He}^+$  bombardment occurring during the repeated ISS scans used in TD-ISS. To probe the rate of Pt loss by sputtering, an experiment was made on a separate adsorbate-free  $\text{Pt}_7/\text{alumina}$  sample, held at constant temperature, while taking a series of ISS spectra. The rate of Pt ISS signal decrease is indicated in Figure 4 by the dashed line labeled “Pt signal loss from sputtering”. Conversely, for a diborane-covered  $\text{Pt}_7/\text{alumina}$  sample held at 110 K, the Pt signal slowly increased during successive ISS scans due to sputtering of adsorbates initially bound on top of the clusters, as indicated by the line labeled “Pt signal recovery from  $\text{B}_2\text{H}_6$  sputtering”. The Al and O ISS signals were not observed to change significantly in either control experiment, presumably because the diborane coverage on alumina is low, and sputtering of Al or O from the top layer simply exposes more Al and O in the second layer.

As shown in Figure 4, the Pt ISS signal starts to recover significantly faster than would be expected from  $\text{B}_2\text{H}_6$  sputtering at  $\sim 200$  K, gradually recovering to  $\sim 95\%$  of the



**Figure 6.** MD trajectories of diborane decomposition on prismatic Pt<sub>7</sub> reveal that diborane may either split apart to form a B–O<sub>surf</sub> anchor or maximize Pt–B bonds by adsorbing onto a Pt cluster facet. The prismatic structure can also distort significantly or form a flattened, single-layer geometry. At 450 K, beyond 3.0 ps, the cluster changed very little with only the hydrogens translating from one atom to the next or H<sub>2</sub> diffusing through the vacuum gap. Each MD time step corresponded to 1 fs.

adsorbate-free value by ~550 K and then is constant at higher temperatures. The Al and O signals remain attenuated up to ~450 K but then recover to their adsorbate-free values by 700 K.

To summarize, TD-ISS shows that diborane preferentially adsorbs to the Pt<sub>7</sub> clusters at 130 K, and some or all of the Pt-associated diborane is bound at sites on top of the cluster. The small attenuation of the Al and O signal indicates that diborane also binds at sites around the periphery of the cluster or at sites on the alumina film isolated from the clusters or both. Because XPS shows that some boron remains on the support after heating, the gradual recovery of the Pt signal suggests that the boron moves to sites below the Pt clusters.

**DFT Results for Adsorption of Diborane on Pt<sub>7</sub> Clusters.** PW-DFT calculations were performed to identify low-energy adsorption geometries for diborane on Pt<sub>7</sub>/alumina, as summarized in Figure 5. We previously reported on the energetics and geometries of numerous isomers of Pt<sub>7</sub> and Pt<sub>8</sub> bound to alumina.<sup>14</sup> Here, we focus on adsorption of diborane on the two lowest energy minima of Pt<sub>7</sub>/alumina, which are shown in the small figures next to the titles of each section of Figure 5. The most stable Pt<sub>7</sub>/alumina structure is prismatic ( $E_{\text{ads}} = -5.09$  eV, relative to alumina + gas phase Pt<sub>7</sub>), but there is a single-layer isomer that is only slightly higher in energy ( $E_{\text{ads}} = -5.04$  eV). Seven different isomers of diborane adsorbed on both prismatic and single-layer Pt<sub>7</sub>/alumina are shown, all of which would contribute to the population at 700 K and below, according to Boltzmann statistics. In these 0 K, *in vacuo* calculations, the most stable configurations of diborane on the prismatic Pt<sub>7</sub> cluster preserve the B–B bond and are adsorbed atop or peripherally to the cluster. On single-layer Pt<sub>7</sub>, however, the most stable structures involve B–B bond scission.

There are several factors to bear in mind in comparing theory to experiment. Because of computational limits, our DFT calculations were restricted to adsorption of only a single diborane and focused on the strongest diborane binding sites,

i.e., diborane binding on the clusters. The experimental diborane coverages were higher and populated binding sites on both Pt<sub>7</sub> and the alumina film. As a result, the calculations cannot address complex chemistry such as higher borane formation and desorption. In addition, while the minima found by DFT clearly illustrate a variety of binding arrangements, we cannot guarantee that they represent all possible low-energy binding geometries. Indeed, the fluxionality of these clusters is important in their catalysis but also resists facile theoretical description.<sup>6,14,43–46</sup> The complexity of the problem will certainly increase at elevated temperatures or for increasing coverage of B<sub>2</sub>H<sub>6</sub>.

For prismatic Pt<sub>7</sub>/alumina, the most stable isomer in the absence of adsorbates, diborane adsorbs atop or at peripheral sites on the cluster. The B–B bond is preserved with only one or two H atoms transferred from diborane to Pt sites. The B–B bond lengths range from 1.72 to 1.88 Å, compared to 1.76 Å calculated for gas-phase diborane (Figure S6), in excellent agreement with the experimental value (1.7645 Å).<sup>47</sup> Relative to prismatic Pt<sub>7</sub>/alumina + gas phase B<sub>2</sub>H<sub>6</sub>, the most stable binding geometry for diborane on prismatic Pt<sub>7</sub> has  $E_{\text{ads}} = -1.94$  eV, and the other structures shown are all within 0.2 eV ( $\Delta E_{\text{ads}}$ ). The atomic charges for the various isomers of diborane adsorbed on prismatic Pt<sub>7</sub>/alumina are shown in Figure S7.

Diborane binds more strongly to the single layer Pt<sub>7</sub>/alumina isomer, with  $E_{\text{ads}} = -3.22$  eV for the most stable structure. Note that three of the seven isomers shown involve B–B bond scission, and other isomers feature a B–B bond elongated by 7–14% compared to gas-phase B<sub>2</sub>H<sub>6</sub>. All isomers involve transfer of up to three H atoms from B to Pt sites. The atomic charges for the various isomers of diborane adsorbed on single layer Pt<sub>7</sub>/alumina are shown in Figure S8.

The substantially higher  $E_{\text{ads}}$  for diborane on the single-layer Pt<sub>7</sub> isomer implies that with one diborane adsorbed single-layer Pt<sub>7</sub>/alumina becomes the global minimum by ~1.2 eV. The barrier height for diborane-induced isomerization from the

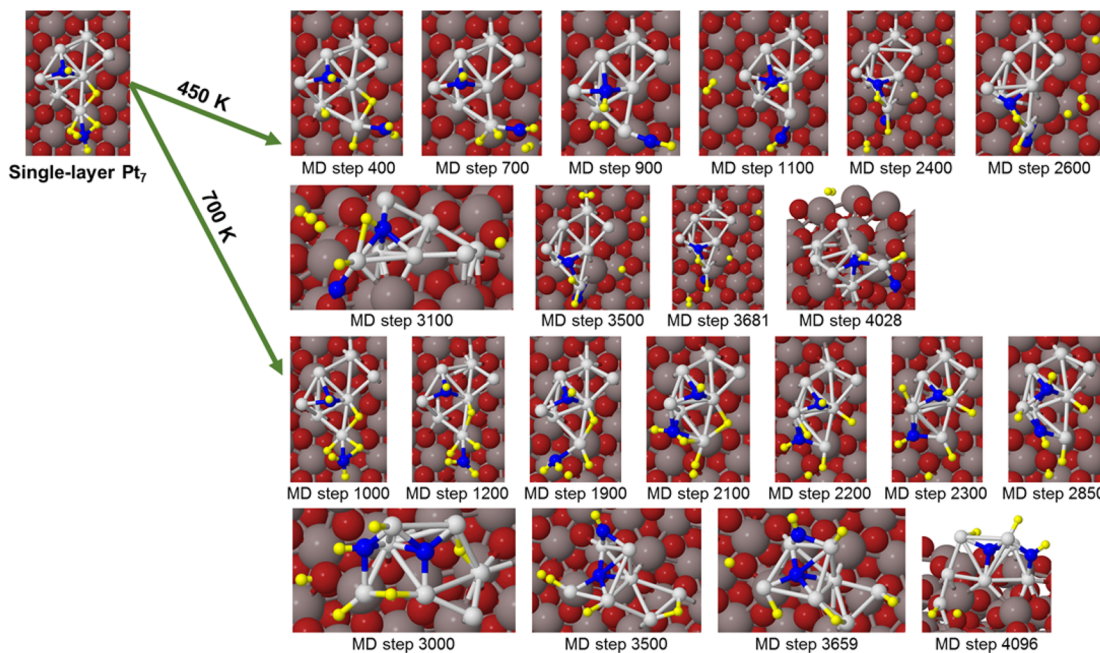


**Figure 7.** MD trajectories of the decomposition of diborane on single-layer  $\text{Pt}_7$  reveal similar bonding trends to prismatic  $\text{Pt}_7$ . The stability of the single-layer structure observed in ground state calculations is retained during MD trajectories at these elevated temperatures of 450 and 700 K. At 450 K, MD steps >3100 resemble MD step 2600. Angled side views of the system at MD steps 3100 and 4028 were taken into highlight the  $\text{B}-\text{O}_{\text{surf}}$  anchor. Each MD time step corresponded to 1 fs.

prismatic local minimum to the single-layer global minimum is unknown, but comparison with ethylene adsorption is suggestive. DFT also found that ethylene adsorbed more strongly on single layer  $\text{Pt}_7/\text{alumina}$  ( $E_{\text{ads}} = -1.97$  eV) compared to prismatic  $\text{Pt}_7/\text{alumina}$  ( $E_{\text{ads}} = -1.29$  eV), and in that case, adsorption of three ethylene molecules was sufficient to eliminate the prismatic-to-single-layer isomerization barrier for  $\text{Pt}_7$ .<sup>14</sup> The difference in adsorption energy for diborane on the two  $\text{Pt}_7$  isomers is almost twice as large as the difference for ethylene, suggesting that isomerization is not unlikely at the diborane exposures used in the experiments.

In summary, DFT shows that diborane spontaneously loses H atoms on both the prismatic and single-layer structures of  $\text{Pt}_7$ ; however, B–B bond scission also occurs on the single-layer  $\text{Pt}_7$ . Extensive diborane decomposition would be expected as the adsorption of diborane drives the prismatic-to-single-layer isomerization of the clusters, and as the sample is heated, driving additional processes.

**Molecular Dynamics Simulations of Diborane/ $\text{Pt}_7/\text{Alumina}$  Thermal Chemistry.** To probe adsorbate effects and chemistry at the elevated temperatures used in the experiments, we used Born–Oppenheimer MD simulations to examine the fate of diborane adsorbed on  $\text{Pt}_7$  at 450 and 700 K. Both of these temperatures are well above the range where  $\text{B}_n\text{H}_m$  desorption is observed (Figure 1) and in the range where  $\text{H}_2$  desorption occurs on Pt clusters (Figure S5). This is also the range of interest for ethylene dehydrogenation, which peaks near 450 K for  $\text{Pt}_7/\text{alumina}$  and goes to completion below 700 K.<sup>14</sup> The prismatic and single-layer minima of  $\text{Pt}_7$  represent different initial geometries for diborane to adsorb and react on. Selected highlights from MD trajectories on each structure at both temperatures are given in Figures 6 and 7, respectively (each MD time step corresponds to 1 fs).

Starting with the lowest energy minimum for diborane on prismatic  $\text{Pt}_7$ , MD shows that at these elevated temperatures

diborane undergoes B–B scission to form  $\text{BH}_2$ ,  $\text{BH}_3$ , or  $\text{BH}_4$  fragments, which may then readsorb onto Pt sites (Figure 6). Interestingly, in the 450 K trajectory, diborane dehydrogenated completely with one of the boron atoms moving to a position underneath the  $\text{Pt}_7$  cluster, forming  $\text{Pt}-\text{B}-\text{O}_{\text{surf}}$  bonds and anchoring the cluster to the alumina surface. In contrast, in the 700 K trajectory, the Pt cluster flattened to a triangular, single-layer structure with BH fragments maximizing the number of Pt–B bonds. Throughout the MD trajectories, at both temperatures, hydrogen atoms are mobile, translating to adsorb onto the Pt cluster, to Al and O atoms on alumina, or forming  $\text{H}_2$  (shown desorbing from the surface). Moreover, both the 450 and 700 K MD trajectories favored B–B bond scission early on, within the first 120 fs of the simulation.

Starting with lowest energy isomer of diborane on single-layer  $\text{Pt}_7$ , at either 450 or 700 K, the Pt cluster retains much of its structure with B or  $\text{BH}_y$  fragments making small translations (Figure 7). Similar to the prismatic Pt cluster, at 450 K, diborane's boron atoms either sit on top of the cluster to maximize Pt–B bonds or move below the cluster to form  $\text{Pt}-\text{B}-\text{O}_{\text{surf}}$  anchor bonds. At 700 K, BH fragments sit on the Pt cluster facets, forming 3–4 Pt–B bonds.

Because of computational time limitations, we were only able to run a few trajectories, following the dynamics for ~5 ps. Of course, the MD picture is incomplete and only accesses a small portion of configurational space accessible to our systems. Nonetheless, these MD results give insight into possible decomposition mechanisms of diborane on alumina-supported Pt clusters. One obvious point is that Pt, B, and H atoms are all mobile at these temperatures, consistent with the DFT finding of numerous structures within a few tenths of an electronvolt of the global minimum. By the end of the trajectories, the  $\text{Pt}_7$  clusters remained intact, but most of the initial B–H bonds had broken, with H atoms binding instead to Pt or to O atoms of the support, and some H atoms recombined to form  $\text{H}_2$  seen

# Pt<sub>4</sub>B<sub>4</sub> on α-Al<sub>2</sub>O<sub>3</sub>

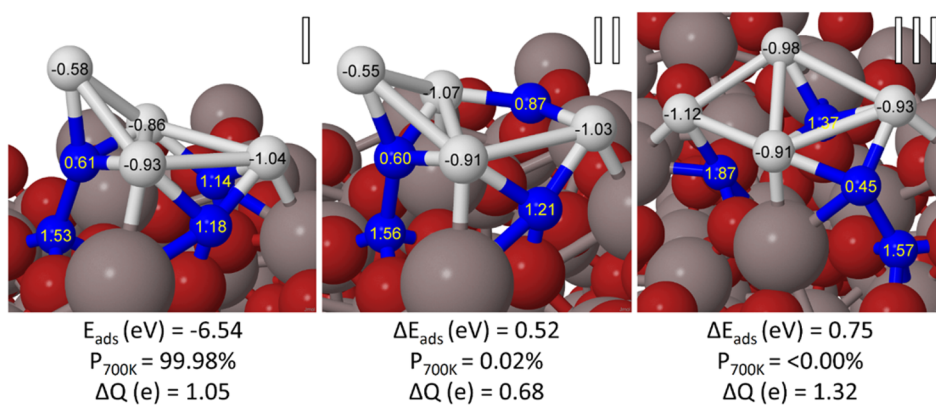


**Figure 8.** Three lowest minima of Pt<sub>4</sub>B<sub>4</sub> adsorbed on alumina with their associated adsorption energies ( $E_{\text{ads}}$ ), Boltzmann populations at 700 K ( $P_{700\text{K}}$ ), and Bader charges on individual atoms. Boron atoms are depicted in blue, platinum in light gray, aluminum in dark gray, and oxygen in red. Isomer II is very similar to isomer I but with a B–O<sub>surf</sub> anchor broken.

desorbing from the surface, even on the relatively short time scale of the trajectory. Boron atoms prefer to bind either under the cluster, forming Pt–B–O<sub>surf</sub> linkages, or to facets of the Pt clusters, forming multiple Pt–B bonds. Boron atoms bound to Pt facets may block preferred carbon adsorption sites or weaken carbon adsorption, which may account for the observed resistance to coking of borated Pt clusters.<sup>4–6</sup> However, B bound between the cluster and the support also affects the affinity to C by altering the electronic structure of the system, particularly the charge transfer from the support to the cluster, as was shown previously.<sup>6</sup>

At the higher diborane coverages of the experiments, additional processes, presumably, would occur, such as coupling of BH fragments to form higher boranes that might desorb (Figure 1) and more extensive recombinative desorption of H<sub>2</sub>. Over longer time scales, particularly at 700 K, additional hydrogen desorption would almost certainly occur, leaving behind Pt<sub>7</sub>B<sub>x</sub> clusters. The simulations suggest that the Pt<sub>7</sub>B<sub>x</sub> clusters would have a range of Pt morphologies (prismatic and single-layer) and boron binding sites (Pt facets, Pt–B–O<sub>surf</sub>), and the cluster structures are likely fluxional at high temperatures.

**Pt<sub>4</sub>B<sub>4</sub>/Alumina.** As a computationally tractable model for Pt<sub>n</sub>B<sub>m</sub> clusters with higher boron mole fraction, as probably form in the experiments, we chose to study Pt<sub>4</sub>B<sub>4</sub> clusters. The global optimization search for gas-phase and adsorbed Pt<sub>4</sub>B<sub>4</sub> was performed utilizing the basin hopping method,<sup>25</sup> and the set of low-energy isomers is shown in Figure 8 and Figure S9 for Pt<sub>4</sub>B<sub>4</sub>/alumina and gas-phase Pt<sub>4</sub>B<sub>4</sub>, respectively. Both gas-phase and adsorbed Pt<sub>4</sub>B<sub>4</sub> structures tend to be (quasi-)planar. Huynh et al. ascribed the drive toward planarity with increasing boron concentration to the covalent nature of boron–boron bonds and boron–metal bonding in mixed metal–boron clusters in B<sub>n</sub>Al<sub>6-n</sub> and LiB<sub>n</sub>Al<sub>6-n</sub> systems and proposed that this effect may be general to other metal–boron systems.<sup>4–6,48</sup> Noticeably, their study found the transition from predominantly 3D to 2D structures occurs when the Al:B ratio is 1:1. The Pt–B clusters seem to follow a similar pattern, with the single-layer geometry dominating in gas-phase Pt<sub>4</sub>B<sub>4</sub> (isomers i–iii, see the Supporting Information) as compared to Pt<sub>7</sub>B (isomers v).<sup>6</sup>

For alumina-supported Pt<sub>4</sub>B<sub>4</sub>, the Pt<sub>4</sub> moiety is also near-planar; however, the B atoms tend to be bent toward the alumina support to allow formation of short B–O<sub>surf</sub> bonds anchoring the Pt<sub>4</sub> moiety to the alumina. The B–B bonds in surface-bound clusters are ~1.7 Å, and Pt–B bonds are ~2 Å. The results also show that even for high boron concentrations, the energetically favorable structures have all the Pt atoms in the surface layer, with most or all of the B atoms underneath the clusters. This has important implications for interpretation of the TD-ISS results and also means that all the Pt atoms are exposed and available to act as catalytic sites.

In previous publications, we predicted that addition of electropositive boron would temper the highly active and electronegative Pt clusters by reducing the charge of the cluster.<sup>6,49</sup> High electron density favors ethylene adsorption in sp<sup>3</sup>-hybridized geometries, a precursor to dehydrogenation. On the other hand, sp<sup>2</sup>-hybridization tends to favor hydrogenation or desorption.<sup>1,3,50–52</sup> In pure Pt<sub>7</sub> and Pt<sub>8</sub> clusters on alumina, Pt atoms were found to have charges ranging from +0.78 e, when bound primarily to O<sub>surf</sub>, to -0.73 e, when bound primarily to Al<sub>surf</sub>, with net cluster charge being ca. -1 e.<sup>14</sup> For Pt<sub>7</sub>B on alumina, the net charge on the clusters dropped to ca. -0.35 e, with strong variations from one isomer to another.<sup>6</sup> With increasing boron content, Pt<sub>4</sub>B<sub>4</sub> clusters on alumina become positively charged, between +0.68 and +1.32 e. In addition, the charge separation between Pt and B atoms increases with increasing boron concentration: Pt remains negative, ranging from -0.5 to -1.1 e, and B atoms are positively charged, between +0.4 e, when forming a mix of Pt–B or B–B bonds within the cluster, and +1.87 e, when forming a B–O<sub>surf</sub> anchor. Increasing the B:Pt ratio also increases the stability of supported Pt–B clusters with Pt<sub>4</sub>B<sub>4</sub> adsorbing more strongly by ~1.9 eV as compared to Pt<sub>7</sub>B ( $E_{\text{ads}} = -4.62$  eV<sup>6</sup>). This may be attributed to the cluster maximizing B–O<sub>surf</sub> interactions and optimizing the electrostatic attraction between the electronegative Pt atoms and electropositive B atoms with a 1:1 ratio of Pt:B.<sup>53</sup>

To summarize the DFT results, we find that diborane spontaneously decomposes on Pt<sub>n</sub>, even at 0 K, and that for high temperatures the decomposition is extensive, generating H<sub>2</sub>, which desorbs even in the short time simulated. Furthermore, there is a tendency for boron atoms to move to

sites under the clusters, forming Pt–B–O bonds that anchor the clusters. This observation is consistent with the ISS observation that the Pt signal recovers substantially after heating, as would be expected if boron moves from the top of the clusters to sites underneath, and hydrogen desorbs.

#### IV. DISCUSSION

From our previous study of ethylene dehydrogenation on borated Pt clusters, we know that boration of Pt<sub>7</sub>/alumina substantially reduces the ethylene desorption temperature, resulting in a significant decrease in the fraction of ethylene that undergoes unwanted dehydrogenation.<sup>6</sup> The obvious questions are how much boron is deposited on the Pt<sub>7</sub>/alumina surface by the boration process used and in what kinds of binding sites is it found.

**Figure 1** shows that quite complex chemistry occurs when diborane is adsorbed on both alumina and Pt<sub>7</sub>/alumina surfaces. The chemistry is qualitatively similar for the two surfaces, reflecting the fact that the Pt<sub>7</sub> coverage is only 10%. Similarities include the low intensity for diborane desorption (mass 26) and higher intensities for desorption of both BH<sub>x</sub> (mass 11) and higher boranes such as tetraborane (mass 48) and pentaborane (mass 59). The fact that desorption is dominated by B<sub>1</sub> or B<sub>n</sub> ( $n \geq 4$ ) species indicates that adsorbed diborane dissociates at low temperatures, undergoing complex recombination chemistry.

The DFT results support this conclusion, showing that even at 0 K diborane spontaneously loses H atoms on both prismatic and single-layer Pt<sub>7</sub> and that on the single-layer isomer B–B bond scission also occurs. Given that the single-layer isomer becomes the global minimum upon diborane adsorption, extensive diborane decomposition is expected. That expectation is supported by the MD trajectory results, in which B–B bond scission and Pt<sub>7</sub> isomerization are observed on the picosecond time scale at moderate temperatures. Experimentally (**Figure S5**) and computationally (**Figure 7**), hydrogen recombinative desorption is observed at moderate temperatures, suggesting that the final state of the borated Pt<sub>7</sub>/alumina samples consists primarily of Pt and B atoms, binding in some fashion to the alumina support.

The XPS results in **Figure 2** show that a significant fraction of the boron initially adsorbed as diborane is left behind after thermal desorption is complete. The amount of boron on the surface can be estimated from XPS peak intensities as detailed in the *Supporting Information*. Because of the low signal-to-noise ratio of the measured B 1s XP spectrum, the calculated boron coverages are estimated to have uncertainties of  $\pm 40\%$ . A detailed analysis aimed at estimating the numbers of B atoms on the surface under different conditions is given in the *Supporting Information*. The main conclusion, consistent with the ISS results, is that a substantial number of diborane molecules adsorb on each cluster, approaching one B<sub>2</sub>H<sub>6</sub>/Pt atom, whereas relatively little diborane binds to the alumina. Heating to 700 K leads to significant loss of boron coverage on alumina; however, essentially all the Pt-bound boron remains on the clusters.

The B 1s binding energies also provide insight into the nature of the binding. Diborane adsorbed at 130 K on Pt<sub>7</sub>/alumina gives rise to a high binding energy peak at 193.9 eV and a broader low binding energy feature that peaks around 189.7 eV. For diborane on alumina, there is a peak at 193.1 eV with similar intensity to that for Pt<sub>7</sub>/alumina, but the signal at low binding energies is much weaker than for the Pt<sub>7</sub>/alumina.

The higher binding energy features are in the energy range (193–193.7 eV) typically reported for fully oxidized boron (B<sup>3+</sup>) in compounds such as boron oxide or boric acid.<sup>54</sup> Elemental boron (B<sup>0</sup>) is reported to have binding energies around 188 eV;<sup>54</sup> thus, the broad 189.7 eV features are suggestive of boron in some partially oxidized form, which obviously is more prevalent when Pt<sub>7</sub> is present. DFT was used to calculate the charges for a single diborane on both prismatic and single layer isomers of Pt<sub>7</sub>/alumina, as shown in **Figures S7 and S8**, respectively. It can be seen that roughly half the boron atoms in the various isomers tend to be fully oxidized (B<sup>3+</sup>), and half are in intermediate oxidation states (B<sup>1.5+</sup> to B<sup>1.6+</sup>). These results appear to be in good agreement with the observed binding energies. It should be noted, however, that for the higher diborane coverages in the experiments higher boranes form on the surface. B 1s binding energies for such species are not known, but we note that an orthocarbonane (B<sub>10</sub>C<sub>2</sub>H<sub>12</sub>) film deposited on copper is reported to have B 1s binding energy of 189.3 eV,<sup>55</sup> also in reasonable agreement with the lower binding energy feature. For reference, in previous studies of low-temperature diborane adsorption/decomposition on Mo(100)<sup>56</sup> and Ni(100)<sup>57</sup> two B 1s peaks were observed at 189.2 and 187.6 eV, but in those experiments the boranes were binding directly to metals, rather than oxides.

After heating to 700 K, both alumina and Pt<sub>7</sub>/alumina samples show a single broad B 1s peak at  $\sim 190.5$  eV, suggesting boron is present in a distribution of intermediate oxidation states. This conclusion is broadly consistent with the distribution of boron oxidation states (B<sup>0.5+</sup> to B<sup>1.9+</sup>) found for B atoms in Pt–B–O<sub>surf</sub> bridge bonds, as shown for Pt<sub>4</sub>B<sub>4</sub> in **Figure 7**.

In summary, XPS indicates that at 130 K diborane adsorbs preferentially in association with Pt clusters, compared to the alumina support, and that little, if any, of this Pt-associated boron desorbs during heating to 700 K. As a result, the boration process investigated leaves Pt clusters with much larger boron coverages than the alumina support. The final B:Pt ratio for the clusters is estimated to be quite high, but we note that the absolute coverages are uncertain by  $\sim \pm 40\%$  due to the very weak B 1s signal. Note also that both the cluster coverage and diborane exposure used in these XPS experiments were twice those for all the other experiments. It is not clear how these changes might have affected the amount of boron deposited *per* cluster; however, we did study how the diborane exposure used in boration affected subsequent ethylene TPD/R. Boration with 0.5 langmuir diborane exposure was found to be almost as effective at suppressing dehydrogenation as boration with 1.5 langmuir exposure; i.e., at least the *chemical effects* of boration appear to saturate at exposures below those used in all the experiments described in this report.

XPS probes boron on the surface, thus providing an indirect method to estimate the fraction that desorbs during heating. TPD/R (**Figure 1**) provides a complementary probe of the desorbing fraction, provided that we can convert the measured B<sub>x</sub>H<sub>y</sub><sup>+</sup> ion signals to fluxes of various neutrals desorbing from the surface. Using a crude approximation discussed in the *Supporting Information*, we can estimate that of the  $\sim 5$  B<sub>2</sub>H<sub>6</sub> molecules found by XPS to be adsorbed at 130 K, the equivalent of  $\sim 0.9$  B<sub>2</sub>H<sub>6</sub>/nm<sup>2</sup> ( $\sim 20\%$ ) desorbs in the form of various boranes, which is in reasonable agreement with the  $\sim 30\%$  desorption estimated from XPS. For Pt<sub>7</sub>/alumina,  $\sim 7$  B<sub>2</sub>H<sub>6</sub>/nm<sup>2</sup> adsorb at 130 K, but only the equivalent of  $\sim 0.80$  B<sub>2</sub>H<sub>6</sub>/nm<sup>2</sup> ( $\sim 11\%$ ) desorb, compared to  $\sim 21\%$  boron

desorption estimated by XPS. Considering the crude approximations required for this analysis, and low XPS signal, the TPD and XPS results are in reasonable agreement regarding the amount of boron lost during heating.

Figures S2 and S3 give the desorption energy distributions for the various borane products observed, all of which are below 0.5 eV. The DFT adsorption energies for diborane on Pt<sub>7</sub>/alumina are all much higher—ranging up to ~3 eV on the single-layer isomer. This discrepancy is easily explained. The DFT calculations were done to find the structure and energetics for a single diborane molecule in the strongest binding sites, which are on the Pt clusters. The experiments were done at much higher diborane coverages and include diborane bound to Pt sites and to the alumina film. As shown by XPS, boron bound to the Pt clusters does not desorb during heating; thus, the TPD/R experiments are only sensitive to boranes desorbing by recombination of B<sub>x</sub>H<sub>y</sub> and H adsorbed on the alumina support, where the binding energies are clearly much lower than for Pt-associated sites.

XPS shows the amount of boron associated with Pt but provides no insight into the nature of the boron–Pt binding. TPD/R gives the temperature ranges in which boranes (Figure 1) and hydrogen (Figure S5) desorb but provides no insight into the sites they desorb from. Analysis of the TD-ISS results (Figure 4) in light of the XPS and TPD data provides some of this structural information. The large attenuation of Pt ISS signal, and much smaller attenuations of Al and O signals, are consistent with the XPS results. Both show that diborane adsorbs more efficiently in association with the Pt clusters than on alumina sites, and ISS shows that a significant fraction adsorbs on top of the clusters where it attenuates Pt signal. Figure 1 shows that desorption of B<sub>n</sub>H<sub>m</sub> species is complete by ~200 K; thus, it is surprising that there is no significant recovery of Pt, O, or Al ISS signals as the sample is heated to 200 K. Recovery of the Pt ISS signal occurs in two stages at higher temperatures. Between 200 and 400 K, the Pt signal increases to about half the expected value for adsorbate-free Pt<sub>7</sub>. This is the temperature range in which hydrogen desorbs from Pt<sub>7</sub> (Figure S5), suggesting that desorption of hydrogen exposed some Pt atoms but that approximately half the Pt atoms remained blocked by adsorbed boron. This conclusion is consistent with the XPS results indicating that little of the boron associated with Pt sites desorbs; i.e., the borane desorption observed in TPD/R originates almost entirely from the alumina film.

Between 400 and 550 K, the Pt signal recovers to almost the adsorbate-free limit. Since nothing desorbs in this temperature range, the recovery of Pt ISS signal must reflect a structural change in the Pt clusters, and the DFT results suggest the explanation. Both the MD simulations (Figures 6 and 7) and the structures found for adsorbed Pt<sub>4</sub>B<sub>4</sub> indicate that the most stable binding sites for boron atoms in Pt<sub>n</sub>B<sub>m</sub> clusters are in Pt–B–O<sub>surf</sub> bridging sites, where the B atoms are under the Pt cluster, anchoring it to the surface. As a result, the Pt atoms are in surface layer and detectable by ISS.

The fact that the Pt ISS signal recovers to 95% of the value for adsorbate-free Pt<sub>7</sub> also suggests that sintering or agglomeration of the clusters during the boration process is limited because either process would tend to form larger, 3D clusters in which a smaller fraction of Pt is in the ISS accessible surface layer. Indeed, the final Pt ISS signal is well above what would be expected from He<sup>+</sup> sputtering of Pt during the series of ISS scans. This, too, is consistent with the XPS results, which

indicate high diborane coverage on the Pt clusters, which would tend to shield the underlying Pt from most of the sputtering that occurs for adsorbate-free clusters.

## V. CONCLUSIONS

We have shown that complex chemistry occurs when diborane is adsorbed on both alumina and Pt<sub>7</sub>/alumina surfaces at low temperatures. Heating to 700 K results in desorption of both BH<sub>x</sub> and higher boranes from the alumina support, with some boron also remaining on the surface, presumably at defects. When Pt clusters are present, the amount of diborane adsorbing is substantially higher, indicating preferential binding at sites associated with the clusters. Diborane is found by DFT to spontaneously decompose on the Pt clusters at 0 K and to undergo extensive decomposition, accompanied by H<sub>2</sub> loss at higher temperatures. Experimentally, little, if any, of the boron associated with Pt is lost, consistent with the DFT findings. This Pt-bound boron is found by DFT, in agreement with TD-ISS, to move to sites beneath the Pt clusters, forming Pt–B–O<sub>surf</sub> bonds that anchor the clusters to the support.

Therefore, we conclude that boration using diborane is a useful strategy for selectively modifying alumina-supported Pt catalysts in ways that may be beneficial. For example, we observe that boron associated with Pt (but not boron simply deposited on the alumina support) reduces the ethylene binding energy, thereby substantially reducing the tendency to undergo dehydrogenation to coke precursors.

## ■ ASSOCIATED CONTENT

### S Supporting Information

The Supporting Information is available free of charge on the ACS Publications website at DOI: 10.1021/acs.jpcc.7b10423.

Details of quantitative estimates; desorption energy distributions (Figures S2–S3), ISS (Figure S4), TPD data (Figures S1, S5); gas phase diborane structure (Figure S6), local minima of gas phase Pt<sub>4</sub>B<sub>4</sub> (Figure S9); clusters with 1 diborane molecule adsorbed (Figures S7–S8) (PDF)

## ■ AUTHOR INFORMATION

### Corresponding Authors

\*E-mail: anderson@chem.utah.edu (S.L.A.).

\*E-mail: ana@chem.ucla.edu (A.N.A.).

### ORCID

Anastassia N. Alexandrova: 0000-0002-3003-1911

Scott L. Anderson: 0000-0001-9985-8178

### Notes

The authors declare no competing financial interest.

## ■ ACKNOWLEDGMENTS

This work was supported by the Air Force Office of Scientific Research under a Basic Research Initiative grant (AFOSR FA9550-16-1-0141) to A.N.A. and S.L.A. M.-A.H. was also funded by the UCLA Graduate Division Dissertation Year Fellowship. CPU resources at the DoD (Department of Defense) High Performance Computing Modernization Program (the US Air Force Research Laboratory DoD Supercomputing Resource Center—AFRL DSRC, the US Army Engineer Research and Development Center—ERDC, and the Navy Supercomputing Resource Center—Navy DSRC), Pacific Northwest National Laboratory's Environ-

mental Molecular Sciences Laboratory's (EMSL) Cascade cluster, Extreme Science and Engineering Discovery Environment's (XSEDE) computing resources, and the UCLA-IDRE cluster were used to conduct this work.

## ■ REFERENCES

- (1) Schulz, H. Short History and Present Trends of Fischer-Tropsch Synthesis. *Appl. Catal., A* **1999**, *186*, 3–12.
- (2) Rahimi, N.; Karimzadeh, R. Catalytic Cracking of Hydrocarbons over Modified Zsm-5 Zeolites to Produce Light Olefins: A Review. *Appl. Catal., A* **2011**, *398*, 1–17.
- (3) Shaikhutdinov, S. K.; Frank, M.; Bäumer, M.; Jackson, S. D.; Oldman, R. J.; Hemminger, J. C.; Freund, H.-J. Effect of Carbon Deposits on Reactivity of Supported Pd Model Catalysts. *Catal. Lett.* **2002**, *80*, 115–122.
- (4) Tan, K. F.; Chang, J.; Borgna, A.; Saeys, M. Effect of Boron Promotion on the Stability of Cobalt Fischer-Tropsch Catalysts. *J. Catal.* **2011**, *280*, 50–59.
- (5) Xu, J.; Chen, L.; Tan, K. F.; Borgna, A.; Saeys, M. Effect of Boron on the Stability of Ni Catalysts During Steam Methane Reforming. *J. Catal.* **2009**, *261*, 158–165.
- (6) Ha, M.-A.; Baxter, E. T.; Cass, A. C.; Anderson, S. L.; Alexandrova, A. N. Boron Switch for Selectivity of Catalytic Dehydrogenation on Size-Selected Pt Clusters on Al<sub>2</sub>O<sub>3</sub>. *J. Am. Chem. Soc.* **2017**, *139*, 11568–11575.
- (7) Rousset, J.; Cadrot, A.; Cadete Santos Aires, F.; Renouprez, A.; Mélinon, P.; Perez, A.; Pellarin, M.; Vialle, J.; Broyer, M. Study of Bimetallic Pd–Pt Clusters in Both Free and Supported Phases. *J. Chem. Phys.* **1995**, *102*, 8574–8585.
- (8) Yang, B.; Khadra, G.; Tuailion-Combes, J.; Tyo, E. C.; Pellin, M. J.; Reinhart, B.; Seifert, S.; Chen, X.; Dupuis, V.; Vajda, S. Temperature-Dependent Evolution of the Oxidation States of Cobalt and Platinum in Co<sub>1</sub>–Xpt Clusters under H<sub>2</sub> and Co + H<sub>2</sub> atm. *J. Phys. Chem. C* **2016**, *120*, 21496–21504.
- (9) Bardotti, L.; Tournus, F.; Albin, C.; Boisron, O.; Dupuis, V. Self-Organisation of Size-Selected Coxpt1-X Clusters on Graphite. *Phys. Chem. Chem. Phys.* **2014**, *16*, 26653–26657.
- (10) Moskovkin, P.; Pisov, S.; Hou, M.; Raufast, C.; Tournus, F.; Favre, L.; Dupuis, V. Model Predictions and Experimental Characterization of Co-Pt Alloy Clusters. *Eur. Phys. J. D* **2007**, *43*, 27–32.
- (11) Kaden, W. E.; Kunkel, W. A.; Anderson, S. L. Cluster Size Effects on Sintering, Co Adsorption, and Implantation in Ir/Sio<sub>2</sub>. *J. Chem. Phys.* **2009**, *131*, 114701–1–15.
- (12) Roberts, F. S.; Kane, M. D.; Baxter, E. T.; Anderson, S. L. Oxygen Activation and Co Oxidation over Size-Selected Ptn/Alumina/Re(0001) Model Catalysts: Correlations with Valence Electronic Structure, Physical Structure, and Binding Sites. *Phys. Chem. Chem. Phys.* **2014**, *16*, 26443–26457.
- (13) Aizawa, M.; Lee, S.; Anderson, S. L. Deposition Dynamics and Chemical Properties of Size-Selected Ir Clusters on TiO<sub>2</sub>. *Surf. Sci.* **2003**, *542*, 253–275.
- (14) Baxter, E. T.; Ha, M.-A.; Cass, A. C.; Alexandrova, A. N.; Anderson, S. L. Ethylene Dehydrogenation on Pt<sub>4,7,8</sub> Clusters on Al<sub>2</sub>O<sub>3</sub>: Strong Cluster Size Dependence Linked to Preferred Catalyst Morphologies. *ACS Catal.* **2017**, *7*, 3322–3335.
- (15) Blöchl, P. E. Projector Augmented-Wave Method. *Phys. Rev. B: Condens. Matter Mater. Phys.* **1994**, *50*, 17953–17979.
- (16) Kresse, G.; Joubert, D. From Ultrasoft Pseudopotentials to the Projector Augmented-Wave Method. *Phys. Rev. B: Condens. Matter Mater. Phys.* **1999**, *59*, 1758–1775.
- (17) Perdew, J. P.; Burke, K.; Ernzerhof, M. Generalized Gradient Approximation Made Simple. *Phys. Rev. Lett.* **1996**, *77*, 3865–3868.
- (18) Kresse, G.; Furthmüller, J. Efficient Iterative Schemes for Ab Initio Total-Energy Calculations Using a Plane-Wave Basis Set. *Phys. Rev. B: Condens. Matter Mater. Phys.* **1996**, *54*, 11169–86.
- (19) Kresse, G.; Furthmüller, J. Efficiency of Ab-Initio Total Energy Calculations for Metals and Semiconductors Using a Plane-Wave Basis Set. *Comput. Mater. Sci.* **1996**, *6*, 15–50.
- (20) Kresse, G.; Hafner, J. Ab Initio Molecular Dynamics for Liquid Metals. *Phys. Rev. B: Condens. Matter Mater. Phys.* **1993**, *47*, 558–561.
- (21) Kresse, G.; Hafner, J. Ab Initio Molecular-Dynamics Simulation of the Liquid-Metal–Amorphous-Semiconductor Transition in Germanium. *Phys. Rev. B: Condens. Matter Mater. Phys.* **1994**, *49*, 14251–14269.
- (22) Bourdillon, A.; El-Mashri, S.; Forty, A. Application of Tem Extended Electron Energy Loss Fine Structure to the Study of Aluminium Oxide Films. *Philos. Mag. A* **1984**, *49*, 341–352.
- (23) Levin, I.; Brandon, D. Metastable Alumina Polymorphs: Crystal Structures and Transition Sequences. *J. Am. Ceram. Soc.* **1998**, *81*, 1995–2012.
- (24) Evans, D. J.; Holian, B. L. The Nose–Hoover Thermostat. *J. Chem. Phys.* **1985**, *83*, 4069–4074.
- (25) Wales, D. J.; Doye, J. P. Global Optimization by Basin-Hopping and the Lowest Energy Structures of Lennard-Jones Clusters Containing up to 110 Atoms. *J. Phys. Chem. A* **1997**, *101*, 5111–5116.
- (26) Boyd, K. J.; Lapicki, A.; Aizawa, M.; Anderson, S. L. A Phase-Space-Compressing, Mass-Selecting Beamline for Hyperthermal, Focused Ion Beam Deposition. *Rev. Sci. Instrum.* **1998**, *69*, 4106–4115.
- (27) Kane, M. D.; Roberts, F. S.; Anderson, S. L. Mass-Selected Supported Cluster Catalysts: Size Effects on Co Oxidation Activity, Electronic Structure, and Thermal Stability of Pd<sub>n</sub>/Alumina (N ≤ 30) Model Catalysts. *Int. J. Mass Spectrom.* **2014**, *370*, 1–15.
- (28) Kane, M. D.; Roberts, F. S.; Anderson, S. L. Effects of Alumina Thickness on Co Oxidation Activity over Pd<sub>20</sub>/Alumina/Re(0001): Correlated Effects of Alumina Electronic Properties and Pd<sub>20</sub> Geometry on Activity. *J. Phys. Chem. C* **2015**, *119*, 1359–1375.
- (29) Chen, P. J.; Goodman, D. W. Epitaxial Growth of Ultrathin Al<sub>2</sub>O<sub>3</sub> Films on Ta(110). *Surf. Sci.* **1994**, *312*, L767–L773.
- (30) Street, S. C.; Goodman, D. W. Chemical and Spectroscopic Studies of Ultrathin Oxide Films. *Chem. Phys. Solid Surf.* **1997**, *8*, 375–406.
- (31) Lai, X.; Chusuei, C. C.; Luo, K.; Guo, Q.; Goodman, D. W. Imaging Ultrathin Al<sub>2</sub>O<sub>3</sub> Films with Scanning Tunneling Microscopy. *Chem. Phys. Lett.* **2000**, *330*, 226–230.
- (32) Wu, Y.; Garfunkel, E.; Madey, T. E. Growth and Oxidation of Ultra-Thin Al Films on the Re(0001) Surface. *Surf. Sci.* **1996**, *365*, 337–352.
- (33) Wu, Y.; Garfunkel, E.; Madey, T. E. Growth of Ultrathin Crystalline Al<sub>2</sub>O<sub>3</sub> Films on Ru(0001) and Re(0001) Surfaces. *J. Vac. Sci. Technol., A* **1996**, *14*, 2554–2563.
- (34) Kane, M. D.; Roberts, F. S.; Anderson, S. L. Alumina Support and Pd<sub>n</sub> Cluster Size Effects on Activity of Pd<sub>n</sub> for Catalytic Oxidation of Co. *Faraday Discuss.* **2013**, *162*, 323–340.
- (35) Yu, J.; Boatz, J. A.; Anderson, S. L.; et al. Borane-Aluminum Surface Interactions: Enhanced Fracturing and Generation of Boron-Aluminum Core-Shell Nanoparticles. *J. Phys. Chem. C* **2017**, *121*, 14176–14190.
- (36) Yeh, J. J.; Lindau, I. Atomic Subshell Photoionization Cross Sections and Asymmetry Parameters: 1 < Z < 103. *At. Data Nucl. Data Tables* **1985**, *32*, 1–155.
- (37) Rabalais, J. W. *Principles and Applications of Ion Scattering Spectrometry: Surface Chemical and Structural Analysis*; Wiley: New York, 2003; p 336.
- (38) Bandiera, J.; Naccache, C.; Mathieu, M. V. Products Formed by the Hydrolysis of Diborane in Contact with  $\Gamma$ -Alumina. *C. R. Acad. Sci., Paris, Ser. C* **1969**, *268*, 901–4.
- (39) Stein, S. E., director Ir and Mass Spectra. In *NIST Chemistry Webbook*, NIST Standard Reference Database Number 69; Mallard, W. G., Linstrom, P. J., Eds.; NIST Mass Spec Data Center, National Institute of Standards and Technology: Gaithersburg, MD, 20899 (<http://webbook.nist.gov>), 2000.
- (40) Chase, M. W., Jr.; Davies, C. A.; Downey, J. R., Jr.; Frurip, D. J.; McDonald, R. A. JANAF Thermochemical Tables, 3rd ed.; *J. Phys. Chem. Ref. Data* **1985**, *14*.
- (41) Fehlner, T. P.; Koski, W. S. Direct Detection of the Borane Molecule and the Boryl Radical by Mass Spectrometry. *J. Am. Chem. Soc.* **1964**, *86*, 2733–2734.

- (42) Kaden, W. E.; Kunkel, W. A.; Roberts, F. S.; Kane, M.; Anderson, S. L. Co Adsorption and Desorption on Size-Selected Pdn/TiO<sub>2</sub>(110) Model Catalysts: Size Dependence of Binding Sites and Energies, and Support-Mediated Adsorption. *J. Chem. Phys.* **2012**, *136*, 204705.
- (43) Zhai, H.; Alexandrova, A. N. Fluxionality of Catalytic Clusters: When It Matters and How to Address It. *ACS Catal.* **2017**, *7*, 1905–1911.
- (44) Gao, M.; Lyalin, A.; Takagi, M.; Maeda, S.; Taketsugu, T. Reactivity of Gold Clusters in the Regime of Structural Fluxionality. *J. Phys. Chem. C* **2015**, *119*, 11120–11130.
- (45) Hakkinen, H.; Abbet, S.; Sanchez, A.; Heiz, U.; Landman, U. Structural, Electronic, and Impurity-Doping Effects in Nanoscale Chemistry: Supported Gold Nanoclusters. *Angew. Chem., Int. Ed.* **2003**, *42*, 1297–1300.
- (46) Xing, X.; Li, X.; Yoon, B.; Landman, U.; Parks, J. H. Dynamic Fluxionality and Enhanced Co Adsorption in the Presence of Coadsorbed H<sub>2</sub>O on Free Gold Cluster Cations. *Int. J. Mass Spectrom.* **2015**, *377*, 393–402.
- (47) Sams, R. L.; Blake, T. A.; Sharpe, S. W.; Flaud, J. M.; Lafferty, W. J. High-Resolution Infrared Study of the N14, N17, and N18 bands Of 1b2h6and10b11bh6. *J. Mol. Spectrosc.* **1998**, *191*, 331–342.
- (48) Huynh, M. T.; Alexandrova, A. N. Persistent Covalency and Planarity in the B N Al<sub>6</sub>–N 2-and Lib N Al<sub>6</sub>–N–(N= 0–6) Cluster Ions. *J. Phys. Chem. Lett.* **2011**, *2*, 2046–2051.
- (49) Dadras, J.; Jimenez-Izal, E.; Alexandrova, A. N. Alloying Pt Sub-Nano-Clusters with Boron: Sintering Preventative and Coke Antagonist? *ACS Catal.* **2015**, *5*, 5719–5727.
- (50) Perry, D. A.; Hemminger, J. C. Σ-Bond Metathesis on a Surface: Dehydrogenation of Cyclohexane on Hydrogen-Saturated Pt (111). *J. Am. Chem. Soc.* **2000**, *122*, 8079–8080.
- (51) Carlsson, A.; Madix, R. The Dynamics of Ethylene Adsorption on Pt (111) into Di-Σ and Π-Bonded States. *J. Chem. Phys.* **2001**, *115*, 8074–8082.
- (52) Stöhr, J.; Sette, F.; Johnson, A. L. Near-Edge X-Ray-Absorption Fine-Structure Studies of Chemisorbed Hydrocarbons: Bond Lengths with a Ruler. *Phys. Rev. Lett.* **1984**, *53*, 1684–1687.
- (53) Ha, M.-A.; Dadras, J.; Alexandrova, A. Rutile-Deposited Pt–Pd Clusters: A Hypothesis Regarding the Stability at 50/50 Ratio. *ACS Catal.* **2014**, *4*, 3570–3580.
- (54) Wagner, C. D.; Naumkin, A. V.; Kraut-Vass, A.; Allison, J. W.; Powell, C. J. NIST X-Ray Photoelectron Spectroscopy Database. NIST Standard Reference Database 20, Version 3.2 (Web Version), 2000.
- (55) Pasquale, F. L.; Kelber, J. A. Site-Specific Electron-Induced Cross-Linking of Ortho-Carborane to Form Semiconducting Boron Carbide. *Appl. Surf. Sci.* **2012**, *258*, 2639–2642.
- (56) Fryberger, T.; Grant, J.; Stair, P. Adsorption of Boron on Molybdenum (100) and Its Effect on Chemisorption of Carbon Monoxide, Ethene, Propene, and 3, 3, 3-Trifluoropropene. *Langmuir* **1987**, *3*, 1015–1025.
- (57) Desrosiers, R. M.; Greve, D. W.; Gellman, A. J. Decomposition of B<sub>2</sub>H<sub>6</sub> on Ni (100). *J. Vac. Sci. Technol., A* **1997**, *15*, 2181–2189.